Air Permeability of Electrospun Polyacrylonitrile Nanoweb

Ramazan Ali Abuzade,[1] Ali Zadhoush,[1] Ali Akbar Gharehaghaji[2]

[1]*Department of Textile Engineering, Isfahan University of Technology, 84156-83111 Isfahan, Iran*
[2]*Department of Textile Engineering, Amirkabir University of Technology, 15875-4413 Teheran, Iran*

Received 21 September 2011; accepted 8 January 2012
DOI 10.1002/app.36774
Published online in Wiley Online Library (wileyonlinelibrary.com).

ABSTRACT: Ultrafine fibers were spun from polyacrylonitrile (PAN) solution in *N*,*N*-dimethylformamide using a homemade electrospinning setup. Fibers with diameter ranging from 80 to 340 nm were obtained. Fiber size and fiber size distribution were investigated for various concentration, applied voltage, and tip-to-collector distance using image analysis. The diameters of the electrospun fibers increase when increasing the solution concentration and decrease slightly when increasing the voltage and needle tip-to-collector distance. Porosity and air permeability are vital properties in applications of electrospun nanofibrous structures. In this study, effects of process parameters on the porosity and air permeability of electrospun nanoweb were investigated as well. Results of statistical analysis showed that solution concentration and applied voltage have significant influences on pore diameters. It was concluded that nanofiber diameter played an important role on the diameter of pores formed by the intersections of nanofibers. A more realistic understanding of porosity was obtained and a quantitative relationship between nanoweb parameters and its air permeability was established by regression analysis. Two separate models were constructed for predicting air permeability in relation to process parameters. Optimization of electrospinning process for producing nanoweb with desirable air permeability is well achieved by these models. The models presented in this study are of high importance for their ability to predict the air permeability of PAN nanoweb both by process or structure parameters. © 2012 Wiley Periodicals, Inc. J Appl Polym Sci 000: 000–000, 2012

Key words: fibers; electron microscopy; gas permeation; modeling

INTRODUCTION

Porosity and air permeability are vital properties in applications such as filtration, fluid barriers, and thermal insulation.[1] Especially, these are taken into consideration in design and engineering of clothing, parachutes sails, vacuum cleaner, fabrics for air bags, and industrial filter fabrics.[2] Apart from clothing aspect, textiles have a wide variety of engineering applications. Textiles go to war, go to space, hold you safely, wrap wounds, go to various sports, etc.[3] Each of these fabrics should have its desirable breath-ability characteristics.

Fibrous materials used for filter media provide advantages of high filtration efficiency and low air resistance.[4] Fibrous structures have found many applications in the protection of human being[5,6] and delicate devices[7] from exposure to hazardous fine particles. They have been the object of intense research, both theoretical and experimental.[8] Nowadays, nonwoven fabrics are finding immense applications in the manufacturing of protective wear fabrics. The advantages of using nonwoven fabrics against the conventional fabrics are low cost, improved barrier properties, impermeability to particulate matter, adequate strength, and comfort properties.

Structural characteristics of nonwovens namely weight, thickness, density, and fiber diameter influence air permeability.[1,2] It was determined that nonwoven fabric weight is an important parameter and has the most dominant effect on air permeability, when compared with thickness, fiber diameter, and density.[9] More recently, there is a growing tendency in the use of micro and nanofibers for engineered fibrous materials, and electrospinning has been the core of this interest.

Electrospinning is one of the processing techniques to spin polymeric fibers with diameter in nanometer scale. Electrospinning is currently the simplest, versatile, applicable, and high potential technique for fabricating continuous nanofibers with diameters down to a few nanometers.[10] In a typical electrospinning setup, a reservoir is used to contain a polymeric solution. The solution is transferred from the reservoir to a spinneret, which is generally a blunt tip needle powered by syringe pump.[11–13] A pendant drop of the polymer solution is allowed to form at the needle tip. A high voltage bias is then applied to the solution such that at a critical voltage,

Correspondence to: A. Zadhoush (zadhoush@cc.iut.ac.ir) or A. A. Gharehaghaji (aghaji@aut.ac.ir).

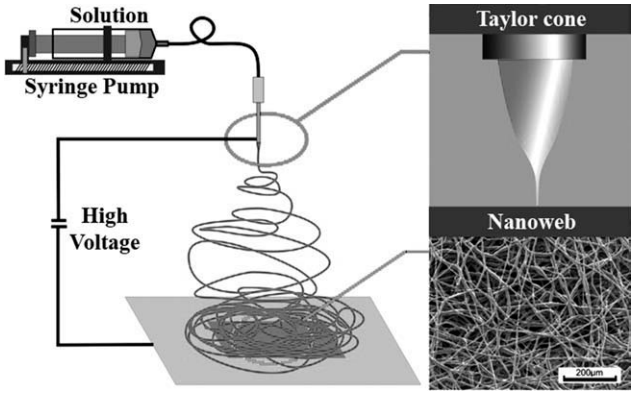

Figure 1 Schematic representation of electrospinning setup.

the electrostatic repulsive forces within the solution will cause a fine jet of solution to erupt from the tip of the pendent drop.[13–15] Although the initial portion of the jet trajectory is stable, it soon enters into a bending instability region where further stretching, bending, spiraling, evaporation of solvent, and looping paths with growing amplitude cause the formation of a nanofibrous nonwoven mesh on collector as shown in Figure 1.[16–26] Due to high porosity and large surface area, polymeric nanofibrous nonwovens are of commercial interest, and they are regarded as favorable candidates for many applications such as filtration membrane and protective clothing.[27]

The air permeability of a textile fabric is determined by the rate of air flow through a material under a differential pressure between the two fabric surfaces.[28] According to ASTM D737, air permeability is defined as the rate of air flow passing perpendicularly through a known area under a prescribed air pressure differential between the two surfaces of a material. The air velocity through pores of the fabric is low, and the fluid flow in the pores is laminar. Darcy's equation demonstrates the normal linear dependence of flow rate with pressure drop for low Reynolds number laminar flows.[29] Darcy's law states that the pressure drop across a porous material is proportional to the flow rate of fluid through it.[30] Equating this sentence, the differential pressure across a fibrous media is expressed by eq. (1):

$$\Delta P = \left(\frac{Q}{A}\right)\left(\frac{\mu}{\kappa}\right)t = K\,\mu V \tag{1}$$

where ΔP is the differential pressure across the fibrous media, Q is the flow rate, A is the sample area, μ is the viscosity of fluid, κ is the permeability of the fibrous media per unit media thickness per unit viscosity, t is the sample thickness, K is the constant of the fibrous media defined as t/κ, and V is the face velocity defined as Q/A. On fibrous webs, thickness measurement is often problematic and can be a large source of error if they are incorporated into reported measurements of Darcy permeability. It is preferred to present the pressure drop/flow rate results in term of an apparent flow resistance defined by eq. (2):

$$R_D = \left(\frac{A\,\Delta P}{\mu Q}\right) \tag{2}$$

where R_D is the apparent Darcy flow resistance.[31]

Although the parameters of the electrospinning process have been well analyzed for many known polymers,[32–38] these information has been inadequate to investigate the efficiency of produced nanoweb in final applications. Hence, a more systematic study is required to be performed to explore the interaction between electrospinning parameters and the efficiency of the nanowebs. This work has studied the effects of electrospinning parameters on the air permeability of electrospun nanoweb.

EXPERIMENTAL

Materials

Industrial polyacrylonitrile (PAN) with average molecular weight ($\overline{M_W}$) of 100,000 g/mol was provided from Poly Acryl Company, Iran. The solvent used was *N*,*N*-dimethylformamide (DMF) from Merck Company, Germany. The concentration from 8 to 20 wt % of PAN/DMF was prepared. The solution was stirred by an electromagnetically driven magnet at a constant rate at 70°C for 2 h. The solution was stored at room temperature, and the experiments were performed at room temperature as well.

Electrospinning

For electrospinning process, the polymer solutions were placed into the syringe to which a capillary tip of 0.21 mm inner diameter was attached. The positive electrode of the high voltage power supply was connected to the capillary tip. The grounded electrode was connected to a rotating drum covered by an aluminum foil, and some paper frames were mounted on it. The polymer solutions in three different concentrations (11%, 13%, and 15%) were electrospun by applying the voltages of 12 and 15 kV at two different tip-to-collector distances of 12 and 15 cm. The flow rate of the polymer solution to the needle tip was maintained by a syringe pump so that a pendant drop remained during electrospinning (2.6–2.8 μL/min). Solutions were electrospun

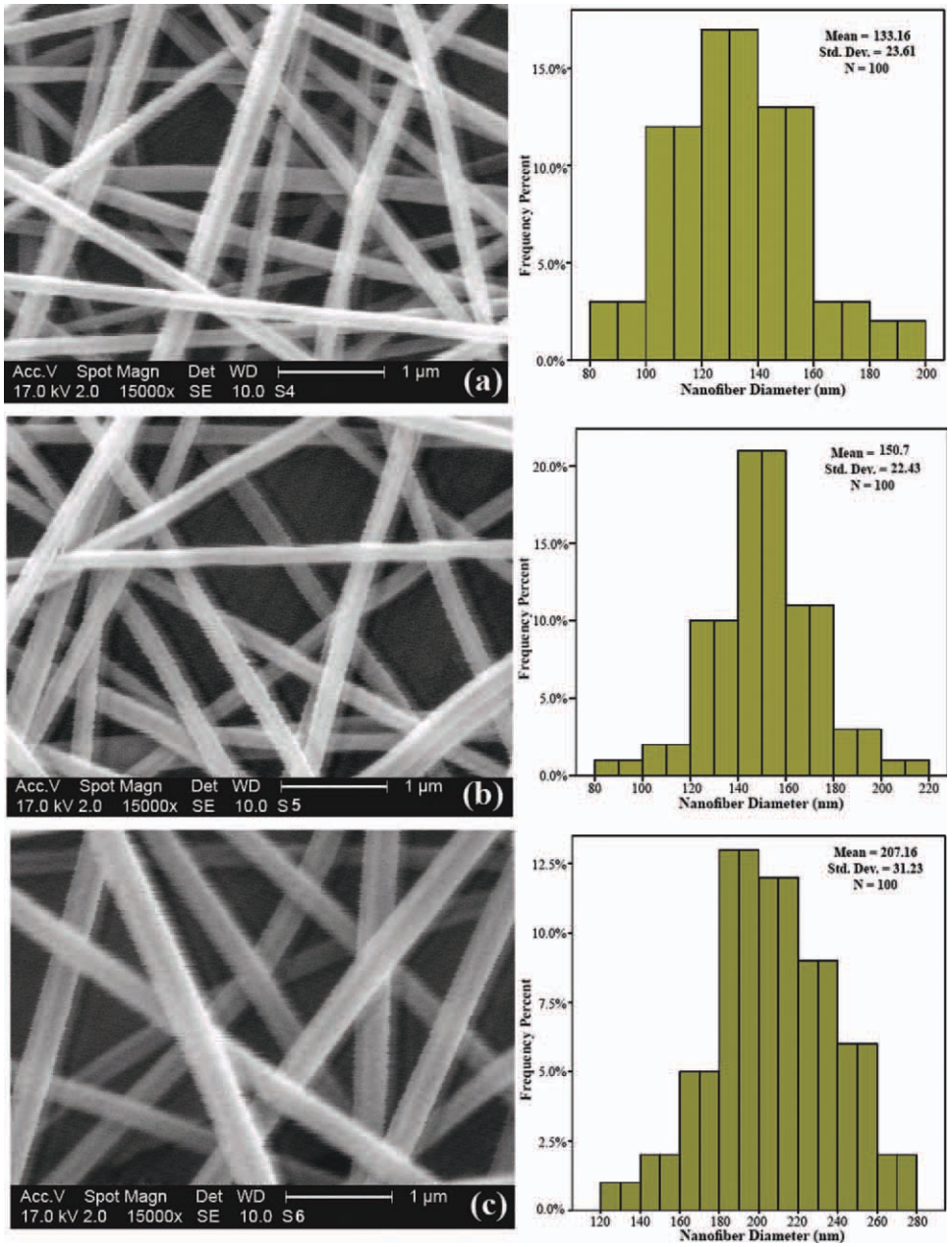

Figure 2 SEM micrographs and size distribution of PAN nanofibers electrospun at polymer concentrations of (a) 11, (b) 13, and (c) 15 wt %, while using spinning parameters at an applied voltage of 15 kV, a distance of 15 cm between the needle tip and collector, and ambient parameters. [Color figure can be viewed in the online issue, which is available at wileyonlinelibrary.com.]

horizontally onto the paper frame and randomly oriented nanofibers were collected.

Characterization

All collected electrospun nanofibers were stored in vacuum for 24 h to ensure that the solvent was vaporized. To determine the structure and porosity of membranes, the nanowebs were characterized with scanning electron microscope (SEM, Philips XL-30 Netherlands). Nanofiber samples were mounted onto SEM plates; sputter coated with gold and inserted in a SEM vacuum vessel for image capturing. The average diameter of the electrospun nanofibers and pores were measured by analyzing SEM images with a custom code image analysis program. On the SEM images, the empty places (voids) were distinguished as separated regions. For each of these regions, the areas were determined by dividing the number of pixels to the resolution of the image. It should be pointed out that the pore shapes are not cylindrical but rather triangular or rectangular. Therefore, a circular equivalent shape with the same area was assumed, and its diameter was considered

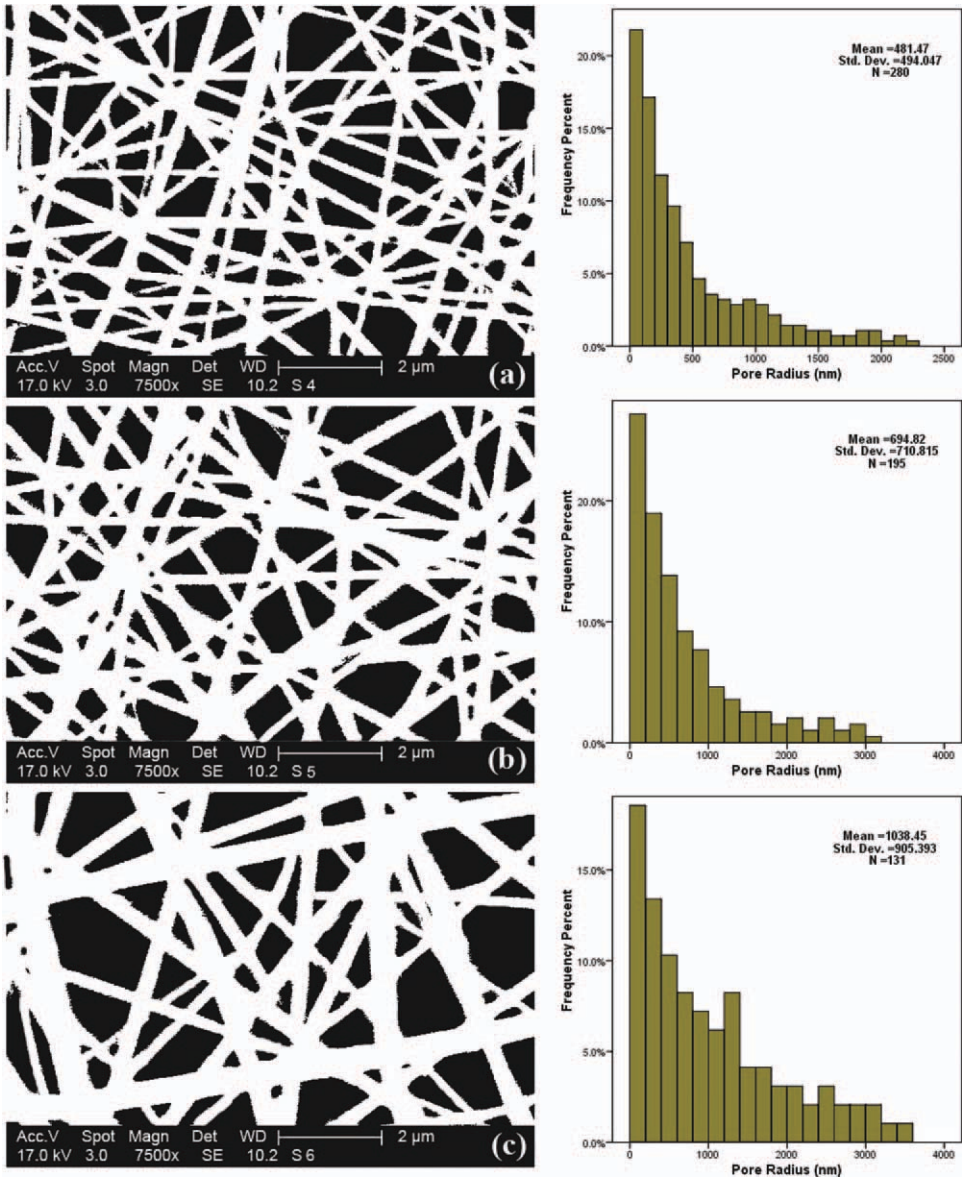

Figure 3 Binary images of SEM micrographs and size distribution of pores for PAN nanofibers electrospun at polymer concentrations of (a) 11, (b) 13, and (c) 15 wt %, respectively, while using spinning parameters at an applied voltage of 15 kV, a distance of 15 cm between the needle tip and collector, and ambient parameters. [Color figure can be viewed in the online issue, which is available at wileyonlinelibrary.com.]

as pore diameter. Finally, the air permeability of nanowebs was measured by a modified tester (M021, SDL International Ltd., North Carolina, USA). All experiments were performed at room temperature following fractional factorial design.

RESULTS AND DISCUSSION

The effect of PAN concentration on the air permeability of electrospun web

Figure 2 show SEM micrographs of PAN nanofibers electrospun at various polymer concentrations and the size distribution of nanofibers diameters. It has been demonstrated by several researchers that the morphology of the nanofibers depends on polymer concentration.[39–43] As it is shown in Figure 2, higher polymer concentration resulted in the more frequent occurrence of courser fibers. The majority of fibers had diameters ranging between 100–160 nm for 11 wt %, 120–180 nm for 13 wt %, and 180–240 nm for 15 wt %. In fact, polymer concentration affects the molecular chain entanglements and the solution viscosity. Hence, the higher polymer concentration leads to more entanglement and less mobility in the chain. This results in lower extension during spinning, producing thicker fibers. In literature, various computer programs are applied to measure porosity and particularly pore size by using SEM images. Similar to Ghasemi-Mobarakeh et al.[44] approach, an

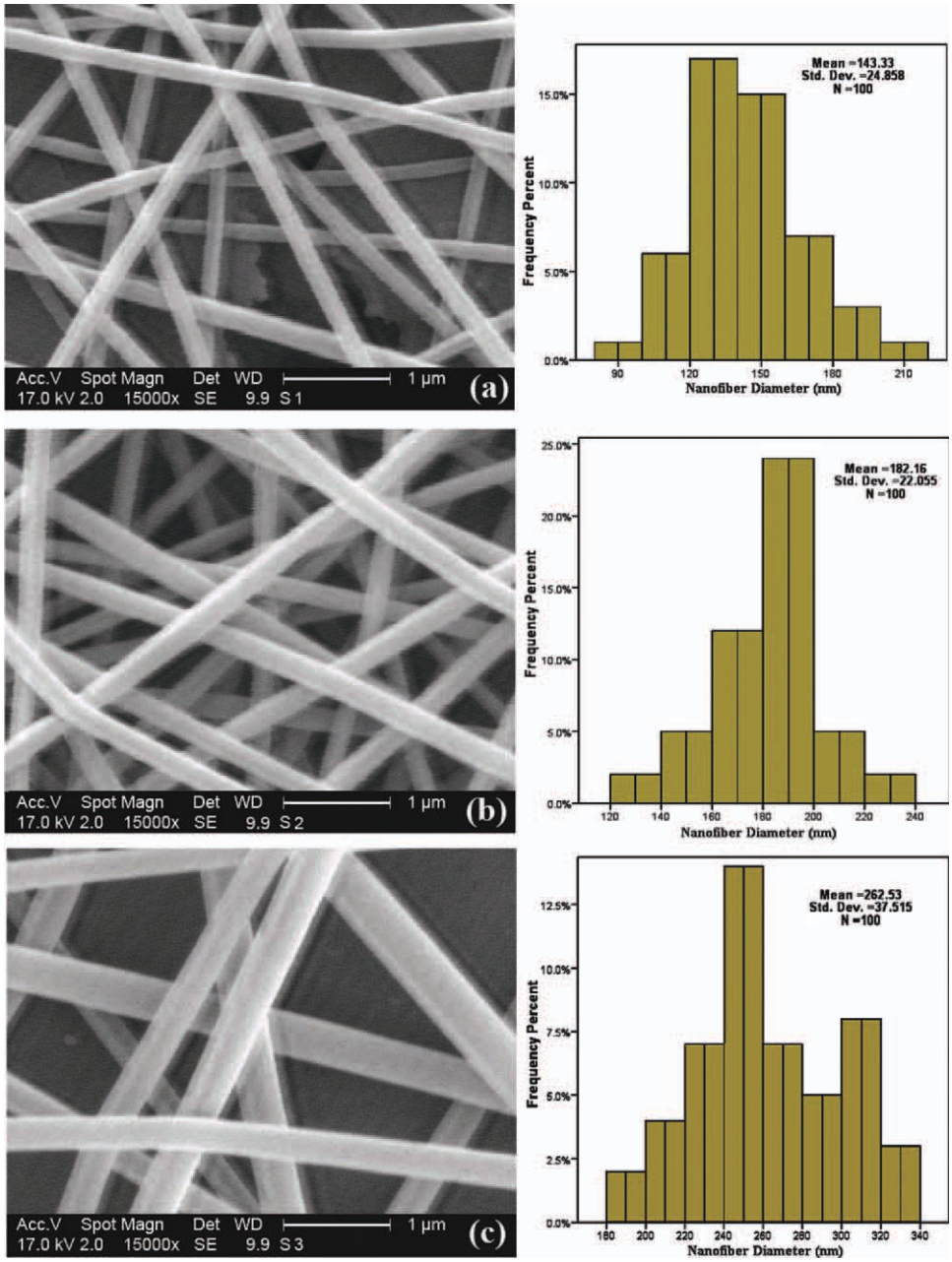

Figure 4 SEM micrographs and size distribution of PAN nanofibers electrospun at polymer concentrations of (a) 11, (b) 13, and (c) 15 wt %, while using spinning parameters at an applied voltage of 12 kV, a distance of 15 cm between the needle tip and collector, and ambient parameters. [Color figure can be viewed in the online issue, which is available at wileyonlinelibrary.com.]

image analysis code was prepared to determine the porosity of the surface layer of nanoweb. In brief, the SEM micrographs of nanoweb were scanned using a scanner (hp scan jet 3670), resolution of scanned images was 600 dpi and gray scale level of 256. This was revealed to be the optimum compromise between rate of analysis and quality of results. After inserting the captured images of SEM pictures to a computer as BMP format of 256 gray scales, image was then converted to a binary form by calculating the threshold. In SEM micrographs of nanoweb, the intensity of pixels in surface layer is higher than that in lower layers. Therefore, the appropriate threshold eliminates lower layers and only the surface layer is obtained. In this surface layer, the empty path may be continuous rather than being tortuous and the tortuosity effect can be neglected. By converting the original image to the binary form, the total pore area, pore size distribution, and porosity percentage can be calculated using the intensity of the pixels of binary images. The binary images of PAN nanofibers electrospun at various polymer

TABLE I
The Results of Porosity and Air Permeation Measurement of PAN Nanoweb

Sample	Porosity (%)	Mean pore radius (nm)	No. of pores	Air permeability per unit web weight[a] $(L/m^2s)/g$
PAN 11 wt % in DMF, 15 kV, 15 cm	59.23	481.5	280	462.3
PAN 13 wt % in DMF, 15 kV, 15 cm	59.40	694.8	195	621.9
PAN 15 wt % in DMF, 15 kV, 15 cm	59.14	1038.4	131	903.2

[a] The results are mean values of five measurements.
Air viscosity, sample area, and pressure drop are the same for all cases.
The air flow rates were normalized to the basis weight of each sample.

concentrations and the results of porosity calculation are shown in Figure 3 and Table I, respectively.

The calculated mean pore sizes are 481 nm for 11 wt %, 694 nm for 13 wt % and 1038 nm for 15 wt %. Pore size increased with polymer concentration. Correlating these results with the nanofiber size distributions of the electrospun webs (Fig. 3), it can be seen that the nanofiber size is the key parameter in determining the pore size of an electrospun nanofiber web. It should be considered that the standard deviation obtained through this method is as high as or higher than the mean pore size reported. But, it is not due to the adopted method and seems to be due to the nature of the phenomenon. It means that other techniques investigating the pore size formed between the electrospun nanofibers result in similar variation. From the statistical point of view, such a variation in measuring a quantity will be troublesome, but in many applications such as filtrations and scaffolds, a range of pore sizes is desirable.

The web morphology has a significant influence on the permeability of air through the webs. Pore characteristics such as porosity, dimension, and size distribution are parameters that directly influence the air permeability of electrospun webs. To investigate the effects of spinning parameters on the air permeability of electrospun nanoweb, the electrospun mats were placed on a circular sample holder of 100 mm in diameters of a manometer (M021, SDL International), and the air flow rate through samples were measured. Based on eqs. (1) and (2), air permeability of the electrospun nanowebs were calculated. As the air viscosity, sample area, and pressure drop remain constant during the tests, airflow rate is a suitable candidate to compare the permeation properties of the samples. To assess the permeation of nanofiber webs in different samples, the measured air flow rates were normalized by the weight of each sample. The air permeability of a nonwoven media is proportional to its thickness indeed. In this work, air permeation data were normalized to the base weight of each sample to avoid any error due to the thickness measurement. The results are shown in Table I.

It is expected that the web with a low porosity should exhibit poorer transport properties. As it can be seen in Table I, there is no significant difference in porosity percent of the three cases, but there are considerable differences between the mean pore size and number of pores in three mentioned cases.

The results of this study showed that higher air permeation is observed at higher concentration polymer solution in the same overall porosity percent. As seen in Table I, the slope of air permeation was increased by increasing the polymer concentration. This can be interpreted that more resistance in air flow through the smaller pores has occurred, which satisfies Poiseuille equation. This states that the volume of a homogeneous fluid passing per unit time through a capillary tube is directly proportional to the pressure difference between its ends and to the fourth power of its internal radius, and inversely proportional to its length and to the viscosity of the fluid as shown by eq. (3)[45]:

$$\Delta P = \frac{8\mu LQ}{\pi r^4} \tag{3}$$

Therefore, at a constant driving pressure the flow rate of air is directly proportional to the fourth power of the radius of the pores and inversely proportional to the length of the pores and viscosity. Hence, higher pore diameter lead to higher air permeation.

The effect of applied voltage on the air permeability of electrospun web

The applied voltages of 12 and 15 kV were adjusted by the high voltage supplier to determine the effect of applied voltage on the electrospun nanoweb morphology and its air permeability. Polymer concentration, feed rate, and distance were kept the same as in the previous section. Figure 4 shows SEM images of electrospun nanofibers produced by adjusting high voltage at 12 kV. Comparing micrographs of Figure 4 with micrographs of Figure 2 (samples produced at 15 kV) showed that the nanofiber diameter

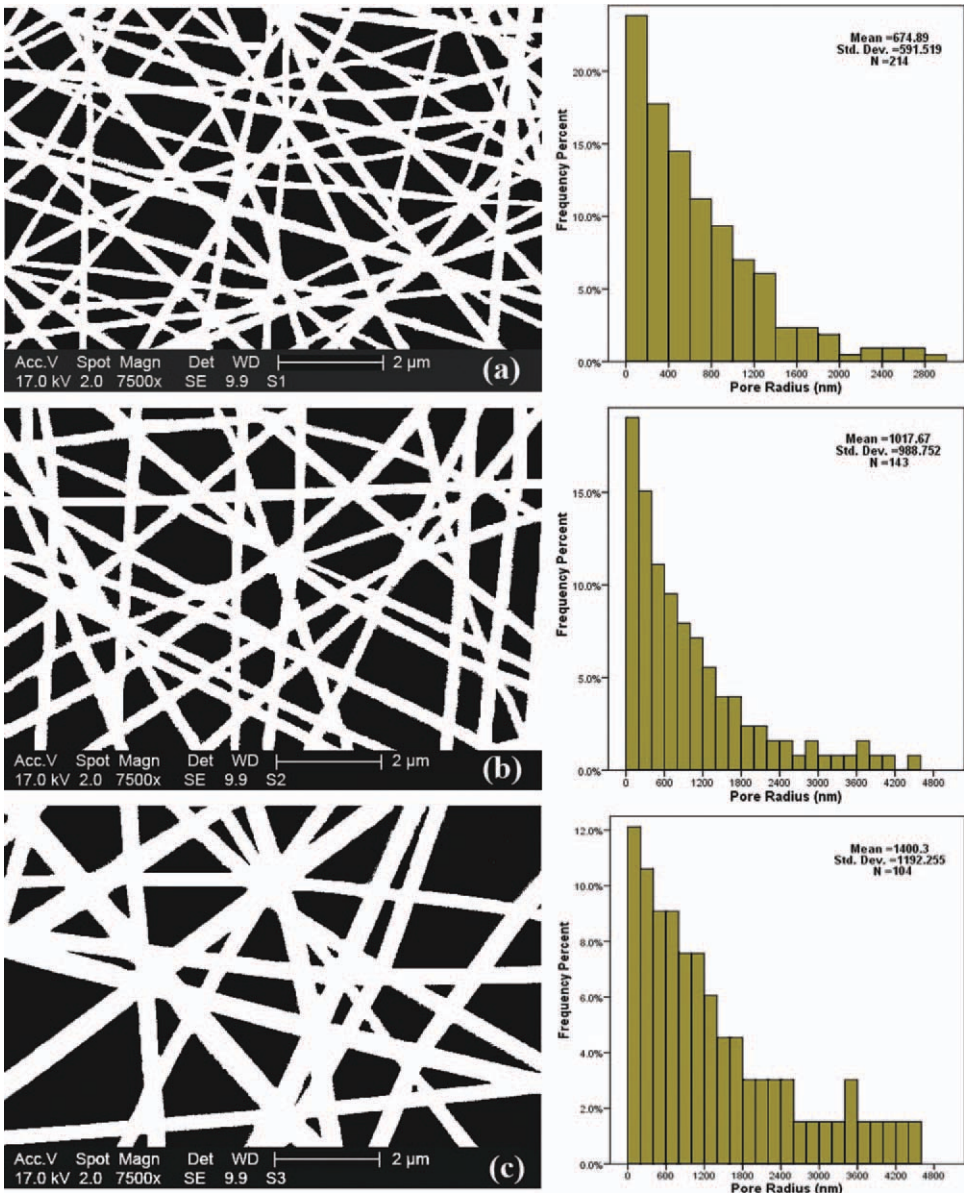

Figure 5 Binary images of SEM micrographs and size distribution of pores for PAN nanofibers electrospun at polymer concentrations of (a) 11, (b) 13, and (c) 15 wt %, respectively, while using spinning parameters at an applied voltage of 12 kV, a distance of 15 cm between the needle tip and collector, and ambient parameters. [Color figure can be viewed in the online issue, which is available at wileyonlinelibrary.com.]

increased with decreasing applied voltage. To clearly observe the difference of fiber size distribution among various samples, the nanofiber size distribution for each case was plotted. In the case of 12 kV, the peak value of nanofiber diameter was in 130, 190, and 250 nm region for 11, 13, and 15 wt % concentration, respectively, and diameter of the majority of the nanofibers was ranged from 100 to 180, 140 to 220, and 220 to 320 nm, respectively. In the case of 15 kV, the number of nanofibers smaller than the peak value was increased even though the peak was located at the same size range with that of the case of 12 kV. In other words, when the applied voltage was 15 kV, much finer nanofibers were generated. The nanofiber diameter peak was in 130, 150, and 190 nm for the aforementioned concentrations, respectively. Distribution of nanofiber diameter followed a normal distribution. It was found that nanofiber diameter tended to decrease with increasing electrospinning voltage, although the influence was not as great as that of polymer concentration. This is in agreement with the results of previous researches.[46,47] The ultra-thin nanofibers obtained in the electrospinning are produced as a result of spiral motion and elongation of a polymer jet driven by a high electrical potential applied between the polymer solution in the capillary and the collector. Those events occur when the repulsive

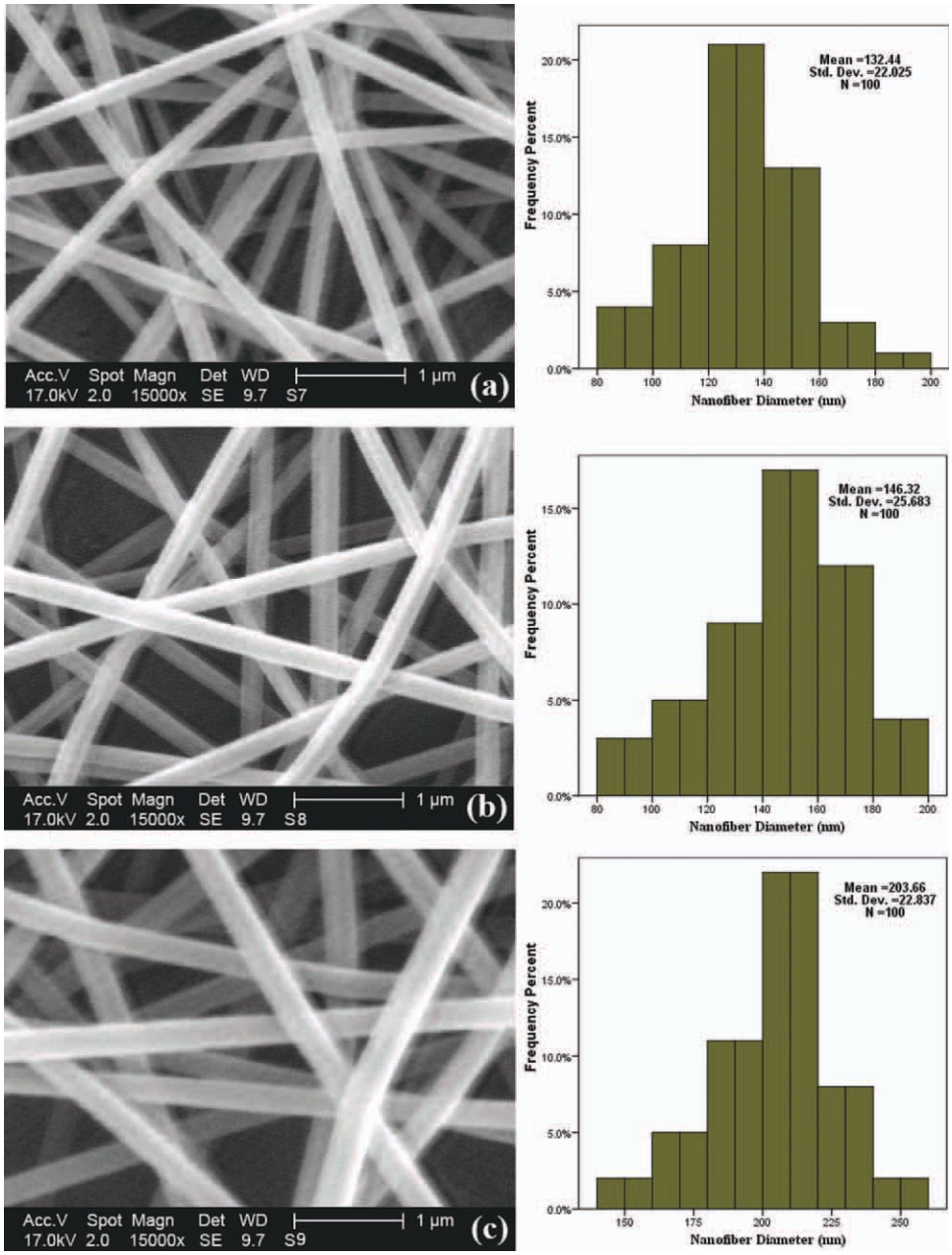

Figure 6 SEM micrographs and size distribution of PAN nanofibers electrospun at polymer concentrations of (a) 11, (b) 13, and (c) 15 wt %, while using spinning parameters at an applied voltage of 15 kV, a distance of 12 cm between the needle tip and collector, and ambient parameters [Color figure can be viewed in the online issue, which is available at wileyonlinelibrary.com.]

electrostatic forces in the polymer jet become large enough to overcome the adhesive force within the jet. In higher electric field, the spiral motion is intensified and facilitates the elongation of a polymer jet in an electrostatic field, which in return leads to finer nanofibers. The peak size of nanofiber diameter was significantly decreased with increasing the electric field. Although it was shown that the diameter of the jet reduced after an initial increase in the field strength, but it should be noted that further increase in field strength will increase the feed rate of the polymer solution through the capillary tip as well. This is one of the complexities of the electrospinning process in which increasing the field strength increases the electrostatic stress and creates finer fibers, but it also draws more materials out of the syringe tend to produce coarser fiber.

The binary images of PAN nanofibers and the results of porosity calculation and permeation tests are shown in Figure 5 and Table II, respectively. The results showed that the mean pore size ranged from 600 to 1400 nm and, as the applied voltage decreased, the pore size increased.

TABLE II
The Results of Porosity and Air Permeation Measurement of PAN Nanoweb

Sample	Porosity (%)	Mean pore radius (nm)	No. of pores	Air permeability per unit web weight[a] (L/m^{2}s)/g
PAN 11 wt % in DMF, 12 kV, 15 cm	50.94	674.9	214	477.7
PAN 13 wt % in DMF, 12 kV, 15 cm	51.32	1017.8	143	560.6
PAN 15 wt % in DMF, 12 kV, 15 cm	51.82	1400.3	104	807.7

[a] The results are mean values of five measurements.
Air viscosity, sample area, and pressure drop are the same for all cases.
The air flow rates were normalized to the basis weight of each sample.

Correlating these results with the nanofiber size distributions of the electrospun webs (Fig. 5), it can be seen that the nanofiber size is the key parameter, which determines the pore size of an electrospun nanofiber web again. An increase in the nanofiber diameter leads to a lower number of pores with

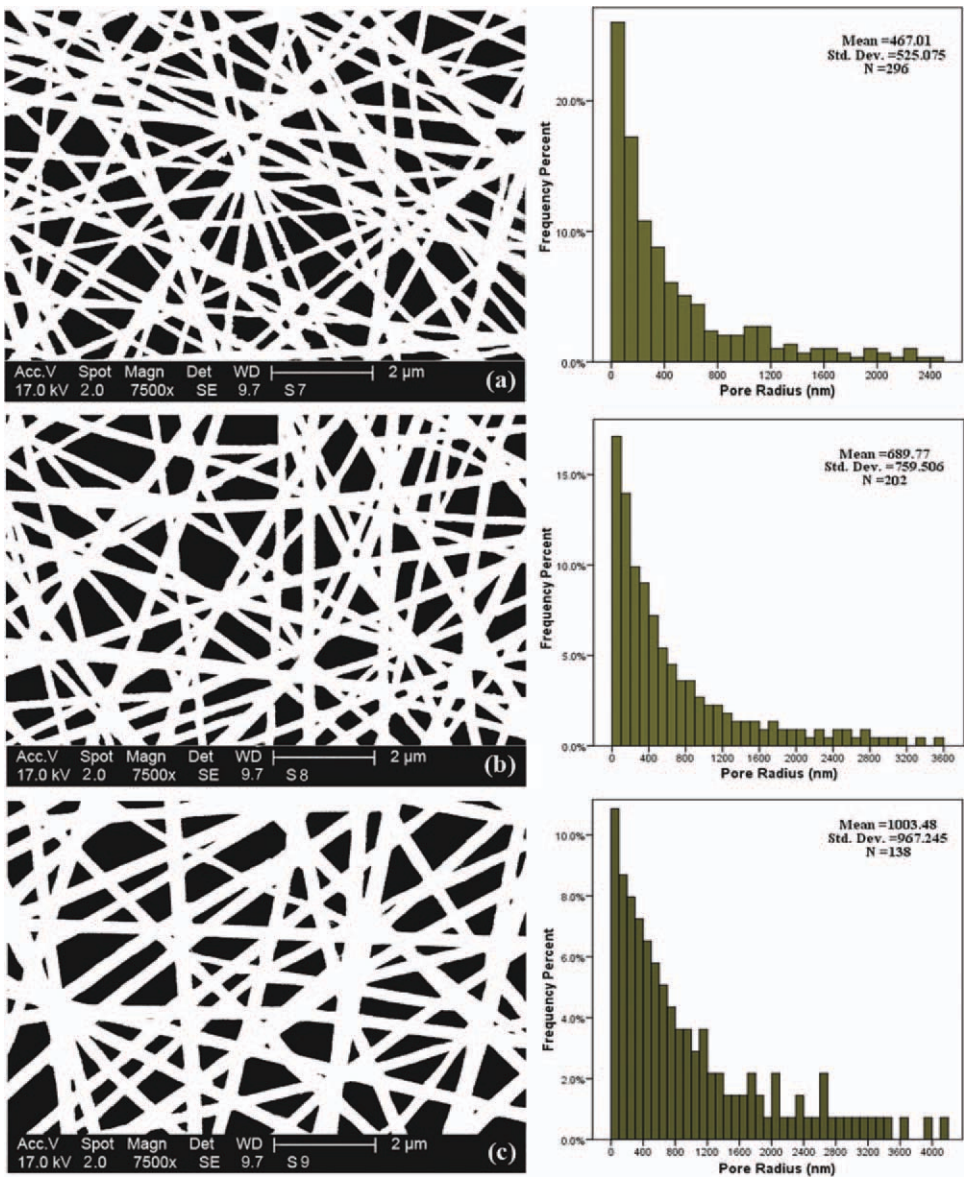

Figure 7 Binary images of SEM micrographs and size distribution of pores for PAN nanofibers electrospun at polymer concentrations of (a) 11, (b) 13, and (c) 15 wt %, respectively, while using spinning parameters at an applied voltage of 15 kV, a distance of 12 cm between the needle tip and collector, and ambient parameters. [Color figure can be viewed in the online issue, which is available at wileyonlinelibrary.com.]

TABLE III
The Results of Porosity and Air Permeation Measurement of PAN Nanoweb

Sample	Porosity (%)	Mean pore radius (nm)	No. of pores	Air permeability per unit web weight[a] (L/m^2s)/g
PAN 11 wt % in DMF, 15 kV, 12 cm	53.34	467.0	296	479.4
PAN 13 wt % in DMF, 15 kV, 12 cm	54.15	689.8	202	631.2
PAN 15 wt % in DMF, 15 kV, 12 cm	54.69	1003.5	138	636.7

[a] The results are mean values of five measurements.
Air viscosity, sample area, and pressure drop are the same for all cases.
The air flow rates were normalized to the basis weight of each sample.

larger dimension. This implies that, keeping constant the porosity percent, the nanoweb permeation will increase, which translates in lower resistance in air flow through the larger pores.

The effect of tip-to-collector distance on the air permeability of electrospun web

The distance between the tip of the needle and the grounded plate was chosen to be 12 and 15 cm to examine the effect of this variable on the morphology and air permeability of electrospun nanowebs. The polymer concentration, applied voltage, and feed rate were kept the same. Figure 6 shows the morphology of electrospun PAN nanofiber manufactured at 12 cm tip-to-collector distance.

The effect of tip-to-collector distance was investigated by comparing the micrographs of Figure 6 with the micrographs of Figure 2. There were not significant differences between average nanofiber diameter and nanofiber size distribution in two cases. At lower tip-to-collector distance, the electric field intensity was greater and reduction of nanofiber diameter is expected, but the solvent did not completely evaporate. The results show that the applied voltage was high enough to eliminate the effect of tip-to-collector distance decrement in this setup. As the nanofiber size was the key parameter in determining the pore size of an electrospun nanofiber web, there were no significant differences between the pore sizes and the permeation properties of the samples produced at 12 and 15 cm tip-to-collector distances. Figure 7 and Table III represent the results of porosity calculation and permeation tests, respectively.

MODELING

Modeling for process parameters

In the previous section of this study, the measured air flow rates for various electrospun nanofiber mats were normalized by the weight of each sample to point out the pure effect of the considered variable such as solution concentration, applied voltage, and tip-to-collector distance. To construct a model based on process parameters, several new tests were performed on a fractional factorial design experiment to fulfill the data requirement for modeling. In this stage, no normalization had been done and the nanofiber mat weight was introduced to the model as an independent variable. Four various concentrations (8, 12, 16, and 20 wt % PAN in DMF), voltages (9, 13, 17, and 21 kV), and tip-to-collector distances (9, 13, 17, and 21 cm) were used, and the mean experimental values of the air permeation for these new electrospun nanowebs were measured and considered.

A multivariable regression model was constructed in which the air permeability was chosen as the dependent variable, and the process conditions including polymer solution concentration, applied voltage, tip-to-collector distance, and nanoweb weight were selected as independent variables. Table IV represents the coefficients of regression model.

TABLE IV
The Coefficients of Regression Model for Air Permeability as a Function of Process Parameters

Model		Unstandardized coefficients		Standardized coefficients		
		B	Std. error	Beta	*t*	Sig.
1	(Constant)	2315.422	950.385		2.436	0.018
	Concentration	247.976	9.575	0.887	25.900	0.000
	Voltage	−17.145	7.143	−0.061	−2.400	0.020
	Distance	2.264	7.106	0.008	0.319	0.751
	Weight	−953.708	249.791	−0.131	−3.818	0.000

Dependent variable: air permeability

TABLE V
The Coefficients of Regression Model for Air Permeability as a Function of Nanoweb Structure

		Unstandardized coefficients		Standardized coefficients		
	Model	*B*	Std. error	Beta	*t*	Sig.
2	Fiber diameter	8.868	0.175	0.957	50.765	0.000
	Porosity	17.088	3.248	0.259	5.261	0.000
	Number of pores	0.539	0.189	0.049	2.857	0.006
	Weight	−203.684	40.137	−0.250	−5.075	0.000

Dependent variable: air permeability

Effect of tip-to-collector distance on air permeability of electrospun nanoweb was observed to be almost negligible, while solution concentration, applied voltage, and nanoweb weight were high. However, the last three variables were found statistically significant for air permeability of electrospun nanoweb as shown by eq. (4):

$$\mathrm{AP} = 247.9\ C - 17.2V - 956.1\ W + 2358.3 \qquad (4)$$

where AP is air permeability $(\mathrm{L}/m^2\ s)$, C is polymer weight concentration, V is applied voltage (kV), and W is the weight of nanoweb (mg). The linear multivariable regression model is able to predict the interactions of the variable on the resultant air permeability. It should be noted that this model is constructed for light nanowebs with few layers in which the effects of tortuosity is negligible. In our next study, the effect of layering on permeability of electrospun nanoweb will be studied in detail.

Modeling for image analysis

Another linear multivariable regression model was built to investigate the effects of nanoweb structure on its air permeability using image analysis. For this purpose, all 64 new samples were studied by SEM and image analysis codes. Finally, a multivariable regression model was constructed in which the air permeability was chosen as the dependent variable, and the web structure properties including porosity, mean fiber diameter, mean pore diameter, number of pores, and nanoweb weight were selected as independent variables. Colinearity diagnostics revealed that the correlation between fiber diameter and pore radius was significant at the 0.01 level (two-tailed), so the pore radius was removed. The constant value was not significant statistically and removed as well. Table V represents the coefficients of new regression model for air permeability.

Combining the effects of various structure parameters indicates that the nanoweb air permeation could be modeled by eq. (5):

$$\mathrm{AP} = 8.9\mathrm{FD} + 17.1P + 0.5\mathrm{N}P - 203.7\ W \qquad (5)$$

where AP is air permeability $(\mathrm{L}/m^2\ s)$, FD is mean fiber diameter (nm), P is porosity percent (%), NP number of pores, and W is the weight of nanoweb (mg).

CONCLUSION

This work was aimed at investigating the effect of electrospinning parameters on the air permeability of the nanowebs. For this purpose, the electrospinning of PAN/DMF was processed and fibers with diameter ranging from 80 to 340 nm were obtained depending on the electrospinning condition. Distribution of fiber diameter, distribution of pore size, porosity, and air permeability of nanowebs were investigated at various concentrations, applied voltages, and tip-to-collector distances.

Linear regression and analysis of variance were performed at the significance level of 0.05 to study the impact of concentration, applied voltage, and tip-to-collector distances on fiber diameter, pores diameter, and air permeability of nanowebs.

The results showed that the average fiber diameter increased with increasing polymer concentration, decreasing applied voltage, and increasing tip-to-collector distance. It was concluded that the nanofiber diameter and size distribution were dominant parameters in controlling the pore sizes formed by nanofiber intersections and air permeability of electrospun polymeric nanowebs.

The presented models are of high importance for their ability to predict the air permeability of PAN nanoweb by process or structure parameters. The first regression model can be used to optimize electrospinning conditions to produce nanoweb with desirable air permeation. In the second regression model, the air permeation of PAN nanowebs can be investigated by using the result of image processing of the SEM micrographs and the weights of nanowebs in the model. It can be concluded that the presented models can predict air permeability with sound accuracy and allowing one to avoid the complexities of experimental work.

References

1. Berkalp, O. B. Fibers Text East Eur 2006, 14, 81.
2. Ogulata, R. T. J Text Apparel Technol Manage 2006, 5, 1.
3. Adanur, S. Wellington Sears Handbook of Industrial Textiles; Technomic Publishing: Lancaster, 1995.

4. Tsaia, P. P.; Schreuder-Gibson, H.; Gibson, P. J Electrostat 2002, 54, 333.
5. Lee, S.; Obendorf, S. K. J Appl Polym Sci 2006, 102, 3430.
6. Lee, S.; Obendorf, S. K. Fibers Polym 2007, 8, 501.
7. Podgorski, A. Nanoparticles Med Environ 2010, 13, 251.
8. Pan, N.; Zhong, W. Text Prog 2006, 38, 1.
9. Kothari, V. K.; Newton, A. J Text Inst 1974, 65, 525.
10. Greiner, A.; Wendorff, J. H. Angew Chem Int Ed Engl 2007, 46, 5670.
11. Li, D.; Xia, Y. Adv Mater 2004, 16, 1151.
12. Burger, C.; Hsiao, B. S.; Chu, B. Annu Rev Mater Res 2006, 36, 333.
13. Zhou, F. L.; Gong, R. H.; Porat, I. Surf Coat Technol 2010, 204, 3459.
14. Xie, J.; Li, X.; Xia, Y. Macromol Rapid Commun 2008, 29, 1775.
15. Agarwal, S.; Wendorff, J. H.; Greiner, A. Polymer 2008, 49, 5603.
16. Reneker, D. H.; Yarin, A. L.; Fong, H.; Koombhongse, S. J Appl Phys 2000, 87, 4531.
17. Huang, Z. M.; Zhang, Y. Z.; Kotaki, M.; Ramakrishna, S. Compos Sci Technol 2003, 63, 2223.
18. Teo, W. E.; Ramakrishna, S. Nanotechnology 2006, 17, R89.
19. Yarin, A. L.; Koombhongse, S.; Reneker, D. H. J Appl Phys 2001, 89, 3018.
20. Katta, P.; Alessandro, M.; Ramsier, R. D.; Chase, G. G. Nano Lett 2004, 4, 2215.
21. Greiner, A.; Wendorff, J. H. Angew Chem Int Ed Engl 2007, 46, 5670.
22. Shin, Y. M.; Hohman, M. M.; Brenner, M. P.; Rutledge, G. C. Appl Phys Lett 2001, 78, 1149.
23. Hohman, M. M.; Shin, M.; Rutledge, G. C.; Brenner, M. P. Phys Fluids 2001, 13, 2201.
24. Sill, T. J.; Von Recum, H. V. Biomaterials 2008, 29, 1989.
25. Subbiah, T.; Bhat, G. S.; Tock, R. W.; Parameswaran, S.; Ramkumar, S. S. J Appl Polym Sci 2005, 96, 557.
26. Li, D.; Wang, Y.; Xia, Y. Nano Lett 2003, 3, 1167.
27. Huang, Z. M.; Zhang, Y. Z.; Kotaki, M.; Ramakrishna, S. Compos Sci Technol 2003, 63, 2223.
28. Epps, H. H.; Leonas, K. K. J Test Eval 1986, 24, 26.
29. Carmen, P. G. Flow of Gases Through Porous Media; Butterworth Scientific Publications: London, 1956.
30. Brown, R. C. Air Filtration, an Integrated Approach to the Theory and Applications of Fibrous Filters; Pergamon Press: Oxford, 1993.
31. Gibson, Ph.; Schreuder-Gibson, H.; Rivin, D. Colloids Surf A 2001, 187–188, 469.
32. Reneker, D.; Chun, I. Nanotechnology 1996, 7, 216.
33. Deitzel, J. M.; Kleinmeyer, J.; Harris, D.; Beck-Tan, N. C. Polymer 2001, 42, 261.
34. Zhang, C.; Yuan, X.; Wu, L.; Han, Y.; Sheng, J. Eur Polym J 2005, 41, 423.
35. Theron, S. A.; Zussman, E.; Yarin, A. L. Polymer 2004, 45, 2017.
36. Gupta, P.; Elkins, C.; Timothy, E. L.; Wilkes, G. L. Polymer 2005, 46, 4799.
37. Subbiah, T.; Bhat., G. S.; Tock., R. W.; Parameswaran, S.; Ramkumar, S. S. J Appl Polym Sci 2005, 96, 557.
38. Huang, C.; Chen, S.; Lai, C.; Reneker, D. H.; Qiu, H.; Ye, Y.; Hou, H. Nanotechnology 2006, 17, 1558.
39. Mun, R. P.; Byars, J. A.; Boger, D. V. J Non-Newtonian Fluid Mech 1998, 74, 258.
40. Shenoy, S. L.; Bates, W. D.; Frisch, H. L.; Wnek, G. E. Polymer 2005, 46, 3372.
41. Jarusuwannapoom, T.; Hongrojjanawiwat, W.; Jitjaicham, S.; Wannatong, L.; Nithitanakul, M.; Pattamaprom, C.; Koombhongse, P.; Rangkupan, R.; Supaphol, P. Eur Polym J 2005, 41, 409.
42. Deitzel, J. M.; Kleinmeyer, J.; Harris, D.; Beck-Tan, N. C. Polymer 2001, 42, 261.
43. Tao, J.; Shivkumar, S. Mater Lett 2007, 61, 2325.
44. Ghasemi-Mobarakeh, L.; Semnani, D.; Morshed, M. J Appl Polym Sci 2007, 106, 2536.
45. Sutera, S. P.; Skalak, R. Annu Rev Fluid Mech 1993, 25, 1.
46. Buchko, C. J.; Chen, L. C.; Martin, D. C. Polymer 1999, 40, 7397.
47. Fong, H.; Chun, I.; Reneker, D. H. Polymer 1999, 40, 4585.